Journal of Solid State Chemistry 183 (2010) 565–574

Contents lists available at ScienceDirect

Journal of Solid State Chemistry

journal homepage: www.elsevier.com/locate/jssc

Ternary systems Sr–{Ni,Cu}–Si: Phase equilibria and crystal structure of ternary phases

Navida Nasir [a], Nataliya Melnychenko-Koblyuk [a], Andriy Grytsiv [a], Peter Rogl [a,*], Gerald Giester [b], Jaroslaw Wosik [c], Gerhard E. Nauer [c]

[a] Institute of Physical Chemistry, University of Vienna, A-1090 Wien, Austria
[b] Institute of Mineralogy and Crystallography, University of Vienna, Althanstrasse 14, A-1090 Wien, Austria
[c] CEST-Kompetenzzentrum für elektrochemische Oberflächentechnologie GmbH Victor-Kaplan-Strasse 2, A-2700 Wr. Neustadt, Austria

ARTICLE INFO

Article history:
Received 23 June 2009
Received in revised form
15 December 2009
Accepted 21 December 2009
Available online 4 January 2010

Keywords:
Phase equilibria
X-ray single crystal and powder diffraction
Crystal chemistry of intermetallics

ABSTRACT

Phase relations were established in the Sr-poor part of the ternary systems Sr–Ni–Si (900 °C) and Sr–Cu–Si (800 °C) by light optical microscopy, electron probe microanalysis and X-ray diffraction on as cast and annealed alloys. Two new ternary compounds $SrNiSi_3$ ($BaNiSn_3$-type) and $SrNi_{9-x}Si_{4+x}$ (own-type) were found in the Sr–Ni–Si system along with previously reported $Sr(Ni_xSi_{1-x})_2$ (AlB_2-type). The crystal structure of $SrNi_{9-x}Si_{4+x}$ (own-type, $x=2.7$, $a=0.78998(3)$, $c=1.1337(2)$ nm; space group $P4/nbm$) was determined from X-ray single crystal counter to be a low symmetry derivative of the cubic, parent $NaZn_{13}$-type. At higher Si-content X-ray Rietveld refinements reveal the formation of a vacant site (□) corresponding to a formula $SrNi_{5.5}Si_{6.5}\square_{1.0}$. Phase equilibria in the Sr–Cu–Si system are characterized by the compounds $SrCu_{2-x}Si_{2+x}$ ($ThCr_2Si_2$-type), $Sr(Cu_xSi_{1-x})_2$ (AlB_2-type), $SrCu_{9-x}Si_{4+x}$ ($0 \le x \le 1.0$; $CeNi_{8.5}Si_{4.5}$-type) and $SrCu_{13-x}Si_x$ ($4 \le x \le 1.8$; $NaZn_{13}$-type). The latter two structure types appear within a continuous solid solution. Neither a type-I nor a type-IX clathrate compound was encountered in the Sr–{Cu,Ni}–Si systems.

Structural details are furthermore given for about 14 new ternary compounds from related alloy systems with Ba.

1. Introduction

Our recent systematic studies have covered phase relations, crystal chemistry, physical and particularly thermoelectric properties of clathrate compounds in the ternary systems Ba–*M*–{Si,Ge} with *M*=Mn, Fe, Co, Pd, Pt, Cu, Zn, Cd. [1–7]. These investigations have also led to the discovery of a family of superconducting skutterudites {Sr,Ba,Eu,Th,U}Pt_4Ge_{12} [8], of a non-centrosymmetric superconductor $BaPtSi_3$ [9] as well as of several new compounds with unique crystal structure: $BaPt_5Si_{12}$ [10] and *EP*$Co_{4.7}Ge_9$ (*EP*=Ba, Sr, Eu) [11]. Besides these findings, further compounds have been discovered in the aforementioned ternary systems, which hitherto have not been completely covered by these publications. This particularly concerns the compounds with composition Ba*M*(Si,Ge)$_3$ (*M*=Pd, Pt, Rh, Ir with $BaNiSn_3$-type structure), BaM_2(Si,Ge)$_2$ (*M*=Zn, Cd with $ThCr_2Si_2$-type structure) and BaM_x(Si,Ge)$_{2-x}$ (*M*=Pd, Pt, Cu, Zn, Cd with AlB_2-type). Therefore, the current article will provide information on the crystal structure of the above mentioned phases in the

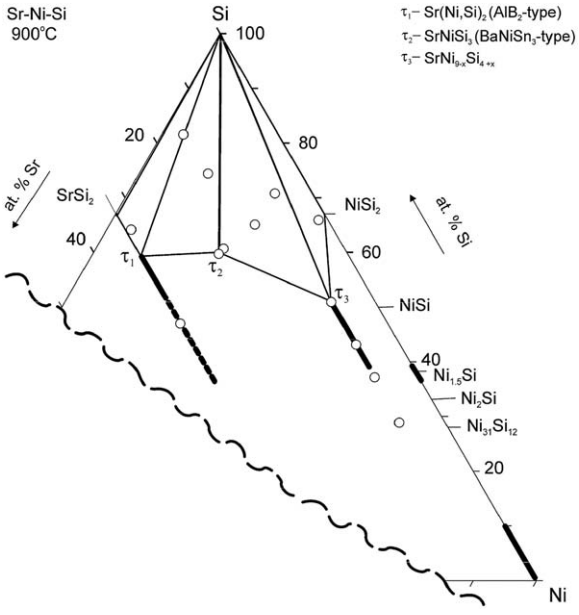

Fig. 1. Partial isothermal section of the Sr–Ni–Si system at 900 °C.

* Corresponding author.
E-mail address: peter.franz.rogl@univie.ac.at (P. Rogl).

0022-4596/$ - see front matter © 2009 Elsevier Inc. All rights reserved.
doi:10.1016/j.jssc.2009.12.023

ternary systems Ba–(Pd,Pt,Ir,Rh,Cu,Zn,Cd)–(Si,Ge). As there are few studies on Sr-systems available in literature, the present article will report on the phase equilibria and crystal structure of compounds in the ternary systems Sr–Ni–Si and Sr–Cu–Si.

2. Experimental

All samples, each of total amounts of ca. 1 g, were prepared in an electric arc furnace under Ti-gettered argon with a non-consumable tungsten electrode on a watercooled copper hearth. The purity of barium and strontium was 99.5 mass%, the purity of metals (Pd, Pt, Ni, Cu, Rh, Ir, Ge and Si) was better than 99.9%. Oxygen sensitive barium and strontium were polished and weighed under cyclohexane. The alloys were remelted three times in order to achieve complete fusion and homogeneity. After melting, alloys were subjected to annealing in evacuated quartz tubes with subsequent quenching in water. Alloys containing Zn and Cd (purity was better than 99.9%) were prepared from elemental ingots by reaction in vacuum-sealed quartz tubes at T=800 °C for 4 days. Afterwards the reaction products were powdered to a particle size below 100 μm and compacted in cylinders by cold pressing in a steel die prior to annealing.

Samples from the systems Sr–{Cu,Ni}–Si were annealed for 15 days at 800 °C (Ni,Cu) and for 7 days at 900 °C (Ni). X-ray powder diffraction (XPD) data from as-cast and annealed specimens were collected with a Guinier–Huber image plate system (Cu-$K\alpha_1$ or Fe-$K\alpha_1$; $8^\circ < 2\theta < 100^\circ$). Precise lattice parameters were calculated by least-squares fits to indexed 2θ-values employing Ge as internal standard (a_{Ge}=0.565791 nm).

Single crystal fragments, suitable for X-ray structure determination were broken from samples with nominal compositions $BaPdGe_3$ $BaPtGe_3$, $BaCd_2Ge_2$ and $SrNi_{9-x}Si_{4+x}$ (x=2.5). Inspection on an AXS-GADDS texture goniometer assured high crystals quality, unit cell dimensions and Laue symmetry of the specimens prior to X-ray intensity data collection on a four-circle Nonius Kappa diffractometer equipped with a CCD area detector and employing graphite monochromated Mo$K\alpha$ radiation (λ=0.071073 nm). Orientation matrix and unit cell parameters for tetragonal symmetry were derived using the program DENZO [12]. No absorption correction was necessary because of the rather regular crystal shapes and small dimensions of the

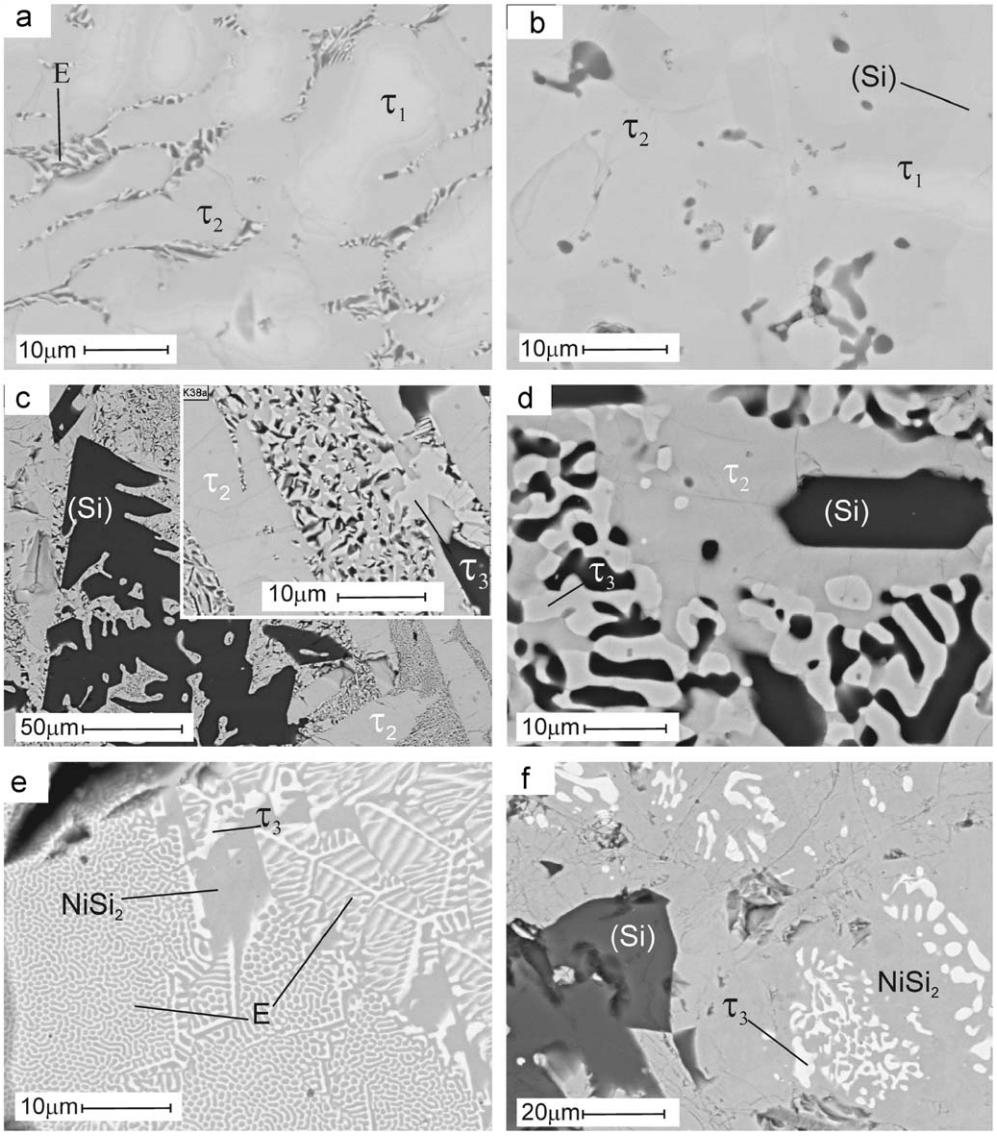

Fig. 2. Microstructure of selected Sr–Ni–Si alloys: (a) $Sr_{20}Ni_{20}Si_{60}$ (as cast), (b) $Sr_{20}Ni_{20}Si_{60}$ 900 °C, (c) $Sr_{12}Ni_{23}Si_{65}$ (as cast), (d) $Sr_{12}Ni_{23}Si_{65}$ (900 °C), (e) $Sr_{1.5}Ni_{32.5}Si_{66}$ (as cast) and (f) $Sr_{1.5}Ni_{32.5}Si_{66}$ (900 °C).

investigated specimens. The structures were solved by direct methods and refined with the SHELXL-97 and SHELXS-97 programs [13].

The as cast and annealed samples were polished using standard procedures and were examined by light optical microscopy (LOM) and scanning electron microscopy (SEM). Chemical compositions for phases were determined via a Philips XL30 field emission environmental scanning electron microscope (ESEM-FEG) operated at 20 kV and equipped with an EDX (Energy Dispersive X-ray) spectrometer supported with Genesis software (USA).

3. Results and discussion

3.1. Phase equilibria in the ternary systems Sr–Ni–Si and Sr–Cu–Si

Sr−Ni−Si: Phase equilibria at 800 °C were found to be similar to those determined after heat-treatment at 900 °C, and therefore the present article reports only the isothermal section at 900 °C (Fig. 1). Three ternary compounds τ_1-Sr(Ni_xSi_{1-x})$_2$ (AlB_2-type), τ_2-$SrNiSi_3$ ($BaNiSn_3$-type) and τ_3-$SrNi_{9-x}Si_{4+x}$ (tetragonal primitive structure related to $CeNi_{8.5}Si_{4.5}$-type) were observed and all these compounds were found to crystallize from liquid. Detailed information on the crystal structure of these phases is available from Section 3.2. The homogeneity region of τ_1-Sr(Ni_xSi_{1-x})$_2$ with AlB_2-type structure extends from 7.0 at% Ni (x=0.10) and continues at least up to 16.0 at% Ni (x=0.34). τ_1 is in equilibrium with $SrSi_2$ and (Si) (as displayed from alloy $Sr_{33}Ni_4Si_{64}$). The solubility of Ni in $SrSi_2$ was <0.5 at%.

The alloy with nominal composition $Sr_{20}Ni_{20}Si_{60}$ evidences primary crystallization of τ_1 (Fig. 2a), followed by secondary peritectic formation of τ_2-$SrNiSi_3$ and a monovariant eutectic (Si)+τ_3 with composition $Sr_{8.6}Ni_{22.1}Si_{69.4}$ (in at%). This eutectic disappears after anneal at 900 °C (Fig. 2b) and the equilibrated alloy consists of three phases $\tau_1+\tau_2$+(Si). Overall composition of this alloy ($Sr_{19.02}Ni_{18.8}Si_{62.17}$) is slightly shifted from the composition of τ_2-$Sr_{20.1}Ni_{20}Si_{59.9}$ (as determined by EPMA), which explains the presence of secondary phases (Si) and τ_1.

The as cast alloy $Sr_{12}Ni_{23}Si_{65}$ shows primary grains of (Si), secondary crystallization of the ternary compound τ_2-$SrNiSi_3$ and a three-phase eutectic $Sr_{16.4}Ni_{17.9}Si_{65.7}$ (in at%) which is composed of τ_2, τ_3 and (Si) (see insert in Fig. 2c) and tends to coarsen after annealing at 900 °C (Fig. 2d). A eutectic with different morphology and composition $Sr_{5.0}Ni_{37.6}Si_{57.4}$ (in at%) is observed in alloy $Sr_{1.5}Ni_{32.5}Si_{66}$ (Fig. 2e): it represents the monovariant crystallization of $NiSi_2$ and τ_3. After annealing at 900 °C a three-phase equilibrium is reached: (Si)+$NiSi_2$+τ_3 (Fig. 2f).

Sr−Cu−Si: The partial isothermal section at 800 °C is shown in Fig. 3. Crystal structures of the ternary phases within the investigated compositional region were found to be consistent with data in literature concerning τ_1-Sr(Cu_xSi_{1-x})$_2$ (x=0.33) ([14], AlB_2-type), τ_2-$SrCu_2Si_2$ ([15], $ThCr_2Si_2$-type) and τ_3-$SrCu_{9-x}Si_{4+x}$ ([16], $CeNi_{8.5}Si_{4.5}$-type). However, tetragonal τ_3-$SrCu_{9-x}Si_{4+x}$ ($0\le x\le 1.0$) undergoes a structural transformation into a cubic structure τ_3'-$SrCu_{13-x}Si_x$ ($1.8\le x\le 4$; $NaZn_{13}$-type; for details see Section 3.2). Thus the as-cast sample with nominal composition $SrCu_9Si_4$ was indexed as a two-phase mixture of tetragonal $CeNi_{8.5}Si_{4.5}$-type (a=0.81339(6) nm and c=1.1620(3) nm) and cubic $NaZn_{13}$-type (a=1.1445(3) nm). After heat treatment at 800 °C for 10 days (i) only the tetragonal phase prevails with lattice parameters a=0.81277(3) nm and c=1.1610(1) nm and (ii) none of the annealed alloys reveals a mixture of cubic and tetragonal structures. As a group–subgroup relation exists between these two structure types, we suggest, that both phases, τ_3-$SrCu_{9-x}Si_{4+x}$ and τ_3'-$SrCu_{13-x}Si_x$, are part of one continuous single-phase region at 800 °C where the homogeneity region of τ_3'-$SrCu_{13-x}Si_x$ extends up to 80.0 at% Cu. This composition at 800 °C was found to be in equilibrium with liquid, and therefore big crystals of τ_3'-$SrCu_{13-x}Si_x$ (x=1.8) and copper-based solid solution (96 at% from EPMA) grew during annealing of the sample at this temperature (Fig. 4a). The liquid crystallizes as a ternary eutectic (insert in Fig. 4a) with composition $Sr_{16.2}Cu_{71.1}Si_{12.7}$ (at%).

The single phase region of τ_2–$SrCu_{2-x}Si_{2+x}$ with $ThCr_2Si_2$-type was found to extend up to ~31.5 at% Cu (x=0.4). The solid solution τ_1-Sr(Cu_xSi_{1-x})$_2$ with AlB_2 type was established to start at $x\ge 0.15$. Rieger et al. [14] reported an AlB_2-type phase at x=0.33, whereas Dörrscheidt and Schäfer [17] investigated the region $0.25\le x\le 0.5$ where they observed a superstructure ($a=2a_o$ and $c=2c_o$). The composition of τ_1 in equilibrium with (Si) and $SrSi_2$ at 800 °C was determined by EPMA from the alloy $Sr_{14.8}Cu_{3.7}Si_{81.5}$. This alloy in as-cast state shows (Fig. 4b) primary dendrites of (Si) and a secondary solidification of τ_1 (9.8 at% Cu after EPMA). A small amount of $SrSi_2$ was determined by XPD but was not observed by SEM. The as-cast alloy $Sr_{20}Cu_{20}Si_{60}$ (nominal composition) shows the crystallization of τ_1 and τ_2 (Fig. 4c). The last liquid crystallizes with formation of τ_3 and a eutectic composed of τ_3 and (Si). After anneal at 800 °C the alloy consists of three phases, τ_1, τ_2 and (Si). The microstructure of the as cast alloy $Sr_{5.9}Cu_{23.5}Si_{70.6}$ shows (Fig. 4d) primary crystallization of (Si) and big dendrites of τ_2 and τ_3 in almost equal amounts. After annealing the sample consists of three equilibrium phases: (Si), τ_2 and τ_3. Joint crystallization of τ_1 and τ_3 along with a small amount of τ_2 is observed in as-cast alloy $Sr_{20}Cu_{40}Si_{40}$ (Fig. 4e). When equilibrated at 800 °C the sample consists of the same phases but with significantly changed volume fractions (Fig. 4f).

Data on composition and lattice parameters for phases coexisting in equilibrium in the ternary Sr−(Ni,Cu)−Si systems are listed in Table 1.

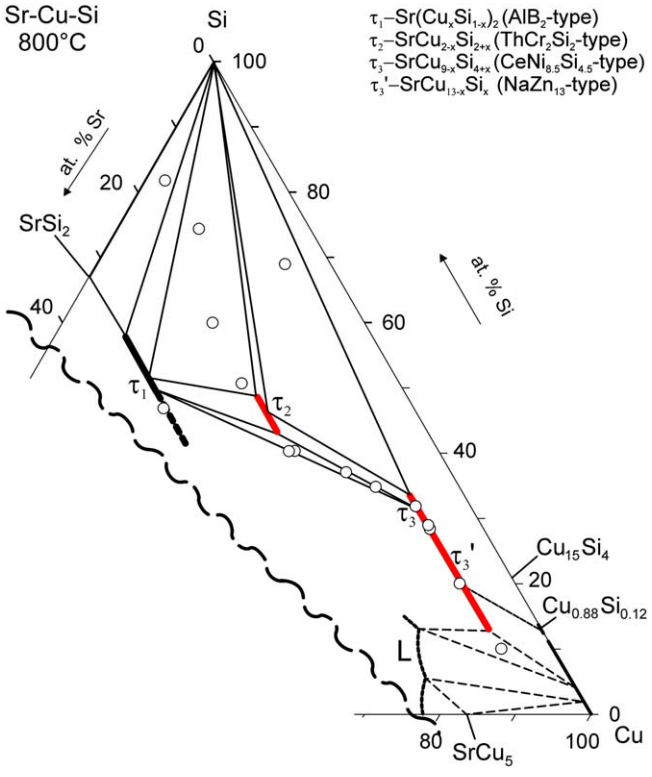

Fig. 3. Partial isothermal section of the Sr–Cu–Si system at 800 °C.

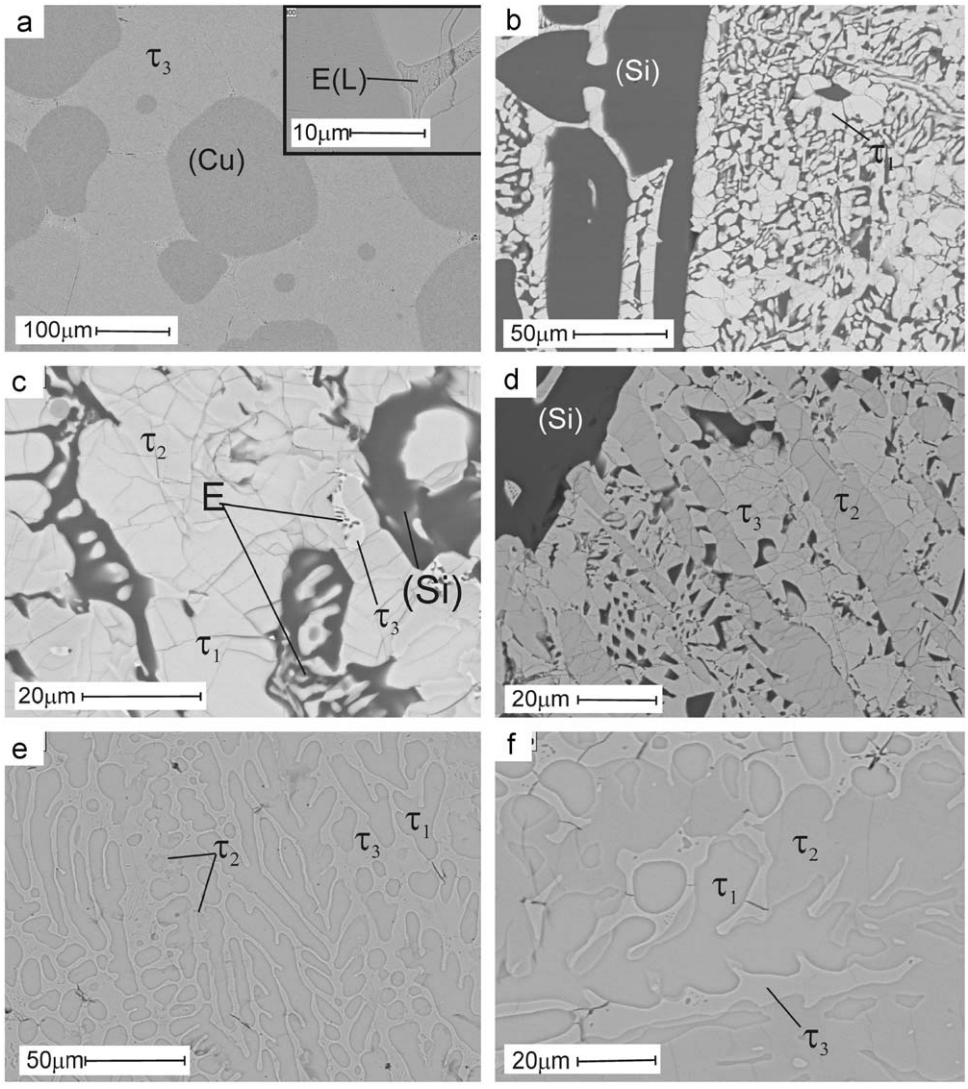

Fig. 4. Microstructure of selected Sr–Cu–Si alloys: (a) $Sr_{7.1}Cu_{83}Si_{10}$ (800 °C), (b) $Sr_{14.8}Cu_{3.7}Si_{81.5}$ (as cast), (c) $Sr_{20}Cu_{20}Si_{60}$ (as cast), (d) $Sr_{5.9}Cu_{23.5}Si_{70.6}$ (as cast), (e) $Sr_{20}Cu_{40}Si_{40}$ (as cast), and (f) $Sr_{20}Cu_{40}Si_{40}$ (900 °C).

Table 1
Three-phase equilibria and lattice parameters for Sr – Ni – Si (900 °C) and Sr – Cu – Si (800 °C) systems.

Phase region	Phase	Composition by EPMA in at%			Lattice parameters	
		Sr	Ni/Cu	Si	*a* (nm)	*c* (nm)
Sr – Ni – Si						
(Si)+$SrSi_2$+τ_1	(Si)	–	–	–	0.54318(2)	–
	$SrSi_2$	–	–	–	0.65370(3)	
	τ_1	32.7	8.3	59.0	0.40564(4)	0.47039(4)
(Si)+τ_1+τ_2	(Si)	–	–	100.0	0.5430	
	τ_1	33.7	7.0	59.3	0.40567(3)	0.46952(7)
	τ_2	20.1	19.7	60.5	0.41958(3)	0.97915(7)
(Si)+τ_2+τ_3	(Si)	97.4	1.5	1.1	0.54308(2)	–
	τ_2	19.7	19.8	60.5	0.41935(5)	0.9793(1)
	τ_3	7.1	42.0	50.8	0.78526(4)	1.1202(2)
(Si)+$NiSi_2$+τ_3	(Si)	100.0	–	–	0.54303(3)	–
	$NiSi_2$	1.7	34.5	63.8	0.54071(4)	–
	τ_3	7.7	43.1	49.2	0.78596(5)	1.1216(2)
Sr – Cu – Si						
(Si)+$SrSi_2$+τ_1	(Si)	–	–	100.0	0.54310(6)	–
	$SrSi_2$	–	–	–		–
	τ_1	33.3	9.8	56.9	0.40759(3)	0.47085(7)

Table 1 (*continued*)

Phase region	Phase	Composition by EPMA in at%			Lattice parameters	
		Sr	Ni/Cu	Si	*a* (nm)	*c* (nm)
(Si)+τ_1+τ_2	(Si)	–	–	100.0		–
	τ_1	33.3	15.6	51.1	0.41079(4)	0.46255(7)
	τ_2	20.0	31.3	48.7	0.41871(5)	1.0022(2)
(Si)+τ_2+τ_3	(Si)	–	–	100.0	0.54292(3)	–
	τ_2	20.0	33.8	46.2	0.41881(1)	1.00267(8)
	τ_3	7.1	58.9	33.9	0.8052(2)	1.158(4)
τ_1+τ_2+τ_3	τ_1	33.3	17.1	49.5	0.41136(2)	0.46228(7)
	τ_2	20.0	36.7	43.3	0.41944(8)	0.9979(2)
	τ_3	7.1	62.2	30.7	0.80994(7)	1.1607(2)

Table 2
Crystal structure for selected ternary compounds in *A*–*T*–*M* systems (*A*=Sr, Ba, *T*=Ni, Cu, Pd, Pt, Zn, Cd, Rh, Ir and *M*=Si, Ge).

Compound	Lattice parameters (nm)		Method	Reference
	a	*c*		
$ThCr_2Si_2$-structure type (*I4/mmm*)				
$BaCd_2Ge_2$	0.46735(6)	1.1448(1)	SC	This work
$BaZn_2Ge_2$	0.45390(3)	1.05279(6)	PD	This work
	0.4527(2)	1.0555(3)	SRRS	[29]
$BaZn_2Si_2$	0.4497(1)	1.02049	SC	This work
$SrCu_{2-x}Si_{2+x}$	0.41907(4)	1.0031(2)	PD	[15]; x=0
	0.41881(5)	1.00267(8)	PD	[This work]; x=0.3
$BaNiSn_3$-structure type (*I4 mm*)				
$BaPdGe_3$	0.45508(4)	1.03649(5)	SC	This work
$BaPtGe_3$	0.45638(8)	1.0231(1)	SC	This work
	0.45636(2)	1.02341(6)	SC	[21]
$BaPdSi_3$	0.43963(3)	1.0186(2)	PD	This work
$BaPtSi_3$	0.44079(2)	1.0017(2)	PD	This work
$BaRhGe_3$	0.45240(3)	1.0274(1)	PD	This work
$BaIrGe_3$	0.45406(1)	1.02132(1)	PD	This work
$SrNiSi_3$	0.41958(3)	0.97915(7)	PD	This work
AlB_2-structure type (*P6/mmm*)				
$Ba(Pd_xSi_{1-x})_2$	0.41950(3)	0.49594(9)	PD	x=0.17; This work
$Ba(Pt_xSi_{1-x})_2$	0.41606(4)	0.50150(5)	PD	x=0.15; This work
$Ba(Cu_xSi_{1-x})_2$	0.41520(8)	0.5058(2)	PD	x=0.19; This work
	0.4117	0.5019	PD	x=0.1; [14]
$Sr(Zn_xSi_{1-x})_2$	0.41639(5)	0.46787(6)	PD	This work
$Sr(Ni_xSi_{1-x})_2$	0.40564(4)	0.47039(4)	PD	x=0.102; This work
	0.4069	0.4663		x=0.25; [30]
$Sr(Cu_xSi_{1-x})_2$	0.40759(3)	0.47085(7)	PD	x=0.15; This work
	0.4108	0.4625	PD	x=0.33; [14]
	0.824(1)	0.921(1)	SC	$0.25 \le x \le 0.5$, a=2a_0; c=2c_0 [17]
$Ba(Cu_xGe_{1-x})_2$	0.4309(2)	0.4965(4)	PD	x=0.29; This work
	0.4616; 0.4312	0.4700; 0.4907		x=0.33, 0.50; [14]
$NaZn_{13}$-related structure types (for details see Tables 5 and 6)				
$SrCu_{13-x}Si_x$	1.15789(8)	–	PD	x=3.6; This work
$SrCu_{9-x}Si_{4+x}$	0.8146(1)	1.1629(2)	SC	x=0; [16]
	0.80722(6)	1.1579(3)	PD	x=1.0; This work
$SrNi_{9-x}Si_{4+x}$	0.78998(3)	1.1337(2)	SC	x=2.7; This work

SC: single crystal, PD: powder diffraction, SRRS: synchrotron radiation resonant scattering.

Table 3
X-Ray single crystal data for $BaPdGe_3$, $BaPtGe_3$ and $BaCd_2Ge_2$ standardized with program *Structure Tidy* [31]. (radiation: Mo$K\alpha$, 2Θ range (°)=$2 \le 2\Theta \le 70$, ω-scans, scan width 2°=150 sec/frame; Total number of frames and sets=411 and 8; Anisotropic displacement parameters (in 10^2 nm^2)).

Parameter/compound	$BaPdGe_3$	$BaPtGe_3$	$BaCd_2Ge_2$
Space group	*I*4*mm*	*I*4*mm*	*I*4/*mmm*
Composition from EPMA	$Ba_{20.0}Pd_{20.0}Ge_{60.0}$	$Ba_{20.6}Pt_{20.5}Ge_{59.0}$	–
Composition from refinement	$Ba_{20.0}Pd_{20.0}Ge_{60.0}$	$Ba_{20.0}Pd_{20.0}Ge_{60.0}$	$Ba_{20.0}Cd_{40.0}Ge_{40.0}$
Formula from refinement	BaPdGe3	$BaPtGe_3$	$BaCd_2Ge_2$
a, *c* (nm)	0.45508(4), 1.03649(5)	0.45638(8), 1.0231(1)	0.46735(6), 1.1448(1)
μ_{abs} (mm^{-1})	33.56	62.49	27.77
V (nm^3)	0.2146	0.2131	0.25004

Table 3 (*continued*)

Parameter/compound	$BaPdGe_3$	$BaPtGe_3$	$BaCd_2Ge_2$
ρ_x (gcm^{-3})	7.1434	11.6013	6.739
Reflections in refinement	$340 \geq 4\sigma(F_o)$ of 341	$324 \geq 4\sigma(F_o)$ of 324	$201 \geq 4\sigma(F_o)$ of 208
Mosaicity	< 0.5	< 0.6	< 0.5
Number of variables	15	15	9
$R_F^2 = \sum \lvert F_0^2 - F_c^2 \rvert / \sum F_0^2$	0.014	0.016	0.021
R_{Int}	0.06	0.07	0.06
wR2	0.033	0.039	0.058
GOF	1.106	1.171	1.155
Extinction (Zachariasen)	0.026	0.019	0.024
Residual density e$^-$/Å^3, max, min	1.10, −1.80	1.96, −2.06	1.53, −2.27
Atom parameters			
Ba in 2*a*(0, 0, *z*), *z*	0.60480(2)	0.59989(6)	Ba in 2*a*(0, 0, 0)
U_{11}=U_{22}, U_{33}	0.0078(1), 0.0074(2)	0.0048(2), 0.0058(3)	0.0102(2), 0.0169(3)
M(Pd/Pt) in 2*a*(0, 0, *z*); *z*	0.24991(6)	0.24690(3)	Cd in 4*d*(0, 1/2, 1/4)
U_{11}=U_{22}, U_{33}	0.0074(1), 0.0073(2)	0.0039(1), 0.0047(2)	0.0143(2), 0.0163(3)
Ge1 in 4*b*(0, 1/2, *z*), *z*	0.35681(6)	0.35324(9)	Ge in 4*e*(0, 0, *z*), 0.38741(6)
U_{11}, U_{22}, U_{33}	0.0118(2), 0.0073(2), 0.0070(2)	0.008(3), 0.0032(3), 0.0059(3)	0.0113(2), 0.0118(3)
Ge2 in 2*a*(0, 0, *z*); *z*	0.0000(1)	0.000(2)	–
U_{11}=U_{22}, U_{33}	0.0092(2), 0.0086(3)	0.0056(3), 0.0069(4)	–
Interatomic distances (nm)	Standard deviation ≤ 0.00004		
Ba– 4Ge2	0.3403	0.3385	Ba– 8Ge 0.35503
–4Ge1	0.3432	0.3399	–8Cd 0.36947
–4Ge1	0.3466	0.3457	Ge– 1Ge 0.25776
–4M	0.3558	0.3565	–4Cd 0.28178
–1M	0.3672	0.3602	–4Ba 0.35503
Ge1– 2M	0.2537	0.2525	Cd– 4Ge 0.28178
–2Ge2	0.2721	0.2729	–4Cd 0.33081
–4Ge1	0.3227	0.3227	–4Ba 0.36947
–4Ba	0.3432	0.3399	
Ge2– 1M	0.2579	0.2539	
–4Ge1	0.2721	0.2729	
–4Ba	0.3403	0.3385	
M– 4Ge1	0.2537	0.2525	
–1Ge2	0.2579	0.2539	
–4Ba	0.3558	0.3565	
–1Ba	0.3672	0.3602	

Table 4
X-Ray powder diffraction data for ternary compounds of (Ba, Sr)−*M*−*X*, (*M*=Rh, Ir, Pd, Pt, Ni, Zn, *X*=Si, Ge) with $BaNiSn_3$ and $ThCr_2Si_2$-type standardized with program *Structure Tidy* [31].

Parameter/compound	$BaIrGe_3$	$BaRhGe_3$	$BaPdSi_3$	$BaPtSi_3$	$SrNiSi_3$	$BaZn_2Si_2$
Space group, Prototype	*I*4*mm*, $BaNiSn_3$	*I*4*mm*, $BaNiSn_3$	*I*4*mm*, $BaNiSn_3$	*I*4*mm*, $BaNiSn_3$	*I*4*mm*, $BaNiSn_3$	*I*4/*mmm*, $ThCr_2Si_2$
Composition, EMPA at%	–	–	$Ba_{20.0}Pd_{20.0}Ge_{60.0}$	$Ba_{19.6}Pt_{20.3}Si_{60.1}$		–
a, *c* (nm), Ge standard	0.45406(1), 1.02132(1)	0.45240(3), 1.0274(1)	0.43963(3), 1.0186(2)	0.44079(2), 1.0017(2)	0.41958(3), 0.97915(7)	0.4497(1); 1.02049
Reflections measured	53	52	50	48	43	51
Θ range	$8 \leq 2\Theta \leq 100$	$8 \leq 2\Theta \leq 100$	$8 \leq 2\Theta \leq 100$	$8 \leq 2\Theta \leq 100$	$8 \leq 2\Theta \leq 100$	$8 \leq 2\Theta \leq 100$
Number of variables	18	24	24	28	24	24
$R_F = \sum \lvert F_o - F_c \rvert / \sum F_o$	0.062	0.057	0.030	0.072	0.045	0.048
$R_I = \sum \lvert I_o - I_c \rvert / \sum I_o$	0.093	0.085	0.046	0.084	0.087	0.062
$R_{wp} = [\sum w_i \lvert y_{oi} - y_{ci} \rvert^2 / \sum w_i \lvert y_{oi} \rvert^2]^{1/2}$	0.071	0.057	0.074	0.086	0.073	0.056
$R_p = \sum \lvert y_{oi} - y_{ci} \rvert / \sum y_{oi}$	0.052	0.044	0.050	0.063	0.047	0.040
$R_e = [N - P + C) / \sum w_i y_{oi}^2)]^{1/2}$	0.027	0.014	0.022	0.019	0.021	0.030
$\chi^2 = (R_{wP}/R_e)^2$	7.13	16.3	11.3	21.3	12.3	3.41
Atom parameters						
Ba/Sr in 2a(0, 0, *z*); *z*	0.5881(2)	0.5897(2)	0.6156(4)	0.5991(9)	0.5984(5)	Ba in 2*a* (0, 0, 0)
B_{iso} (10^2 nm^2)	0.66(3)	0.14(4)	0.62(4)	0.37(6)	0.29(3)	0.9(2)
M in 2a (0, 0, *z*); *z*	0.2385(2)	0.2392(2)	0.2607(4)	0.2477(9)	0.2413(4)	Zn in 4*d* (0, 1/2, 1/4)
B_{iso} (10^2 nm^2)	0.55(2)	0.44(4)	0.06(4)	0.13(4)	0.77(7)	1.1(2)
X1 in 2a(0, 0, *z*); *z*	0.0000(2)	0.0000(3)	0.0000(4)	0.000(2)	0.0000(7)	Si in 4*e* (0, 0, 0.3807(1))
B_{iso} (10^2 nm^2)	1.43(6)	1.52(6)	1.0(1)	1.0(2)	1.7(1)	0.5(3)
X2 in 4b(0, 1/2, *z*); *z*	0.3442(3)	0.3442(3)	0.3702(6)	0.356(1)	0.3530(5)	
B_{iso} (10^2 nm^2)	1.05(4)	0.53(3)	0.48(5)	0.8(1)	0.78(5)	

3.2. Crystal structure of ternary phases

Data on the crystal structure of ternary phases for systems Sr–Cu–Si and Sr–Ni–Si are summarized in Table 2. The table compiles also information on isotypic compounds in ternary systems Ba–*M*–(Si,Ge). All listed compounds belong to three structural families (i) hexagonal AlB_2-type, (ii) tetragonal $BaAl_4$-type ($ThCr_2Si_2$ and $BaNiSn_3$ structure types) and (iii) cubic

$NaZn_{13}$-type (and tetragonal derivative structure types: $CeNi_{8.5}Si_{4.5}$ and $SrNi_{9-x}Si_{4+x}$). Results of the refinements for X-ray single crystal and powder diffraction intensities for these compounds are listed in Tables 3 and 4 showing fine agreement with the assigned prototypes.

Table 5
X-Ray powder diffraction data for $SrCu_{13-x}Si_x$ and $SrCu_{9-x}Si_{4+x}$; anisotropic displacement parameters /temperature factors are in (10^2 nm^2).

Parameter/compound	**$SrCu_{13-x}Si_x$ (x=3.6)**	**$SrCu_{9-x}Si_{4+x}$ (x=1)**
Prototype	$NaZn_{13}$	$CeNi_{8.5}Si_{4.5}$
Space group	$Fm\bar{3}c$	$I4/mcm$
Composition, EMPA at%	$Sr_{7.1}Cu_{61.7}Si_{31.2}$	$Sr_{7.1}Cu_{62.8}Si_{30.1}$
Composition, refinement at%	$Sr_{7.1}Cu_{63.8}Si_{29.0}$	$Sr_{7.1}Cu_{57.1}Si_{35.7}$
a, c (nm), Ge standard	1.15789(8)	0.80722(6), 1.1579(3)
Reflections measured	51	138
Θ range	$8 \le 2\Theta \le 100$	$8 \le 2\Theta \le 100$
Number of variables	27	21
$R_F = \sum \lvert F_o - F_c \rvert / \sum F_o$	0.037	0.054
$R_I = \sum \lvert I_o - I_c \rvert \sum I_o$	0.045	0.078
$R_{wp} = [\sum w_i \lvert y_{oi} - y_{ci} \rvert^2 / \sum w_i \lvert y_{oi} \rvert^2]^{1/2}$	0.061	0.059
$R_p = \sum \lvert y_{oi} - y_{ci} \rvert / \sum y_{oi}$	0.040	0.043
$R_e = [N-P+C) / \sum w_i y_{oi}^2)]^{1/2}$	0.017	0.02
$\chi^2 = (R_{wP}/R_e)^2$	13.2	9.04
Atom parameters		
Sr	Sr 8a (¼, ¼, ¼)	4a (0, 0, ¼)
B_{iso}	0.17(4)	1.28(4)
M1	96i (0, 0.11875(4), 0.18069(4))	16k (0.0594(1), 0.2084(2), 0)
B_{iso}	0.60(3)	1.93(4)
Occ	0.68(2)Cu:0.32Si	1.0 Cu1
Cu2	–	16l (0.6214(1), 0.1214(1), 0.1806(1))
B_{iso}	–	1.75(4)
Si1	–	16l (0.1726(3), 0.6726(3), 0.1149(3))
B_{iso}		1.93(8)
M2	8b (0, 0, 0)	4d (0, 1/2, 0)
B_{iso}	0.67(5)	1.3(1)
Occu.	0.80(2) Cu+0.20 Si	0.99(3)Si

3.2.1. Ternary compounds with AlB_2-type structure (τ_1)

Despite no binary compounds $Sr(Si,Ge)_2$ and $Ba(Si,Ge)_2$ are known with AlB_2-type, this structure type is frequently observed in ternary systems (Sr,Ba)–M–(Si,Ge) (Table 2). A small addition of a third element may stabilize this structure type that appears to be very abundant, particularly in ternary systems with Si. Evidence on an enhanced thermodynamic stability of AlB_2-type phases τ_1 in ternary systems S–(Ni,Cu)–Si follows from the observation of primary crystallization (see for example Fig. 2a) and congruent formation from liquid. The crystal structure of τ_1-$Sr(Cu_xSi_{1-x})_2$ (x=0.15) is confirmed from Rietveld refinements as a simple AlB_2-type as no un-indexed X-ray reflections that may be attributed to superstructures were observed. However, we do not exclude the existence of the superstructure for higher values of x, as reported by [17]. Lattice parameters for the ternary phases with AlB_2 type agree well with values reported in literature.

3.2.2. Ternary compounds with the $BaNiSn_3$-structure type (τ_2)

Single crystals isolated from melted alloys with compositions $BaPdGe_3$ and $BaPtGe_3$ reveal body centered tetragonal unit cells. Structural solutions performed by direct methods were not successful in the highest possible space group $I4/mmm$, however, the structures were resolved in the non-centrosymmetric subgroup $I4\,mm$. Four independent atom positions were found which agree well with the group–subgroup scheme in the Bärnighausen formalism [18,19]. Germanium atoms adopt two crystallographically independent sites 2a (0, 0, z) and 4b (0, $\frac{1}{2}$, z), Pd(Pt) atoms solely occupy the 2a site (0, 0, z) fully consistent with atom order of the $BaNiSn_3$-type [20]. Single crystal refinement data for $BaPdGe_3$ and $BaPtGe_3$ are listed in Table 4 and are consistent with results of [21] for $BaPtGe_3$. X-ray Rietveld refinements for $BaPdSi_3$, $BaPtSi_3$, $BaRhGe_3$, $BaIrGe_3$, $SrNiSi_3$, found in corresponding ternary systems, confirm isotypism with the $BaNiSn_3$-type (Table 4).

Interatomic distances for all these compounds agree well with the sum of atomic radii for exception of relatively short bonds M–Ge1(Si1) and M–Ge2(Si2) (Table 3). Such observation for $BaPtGe_3$ was attributed [21] to strong Pt–Ge interaction. However, such "short" distances are typical for almost all binary M–Ge and M–Si compounds [22].

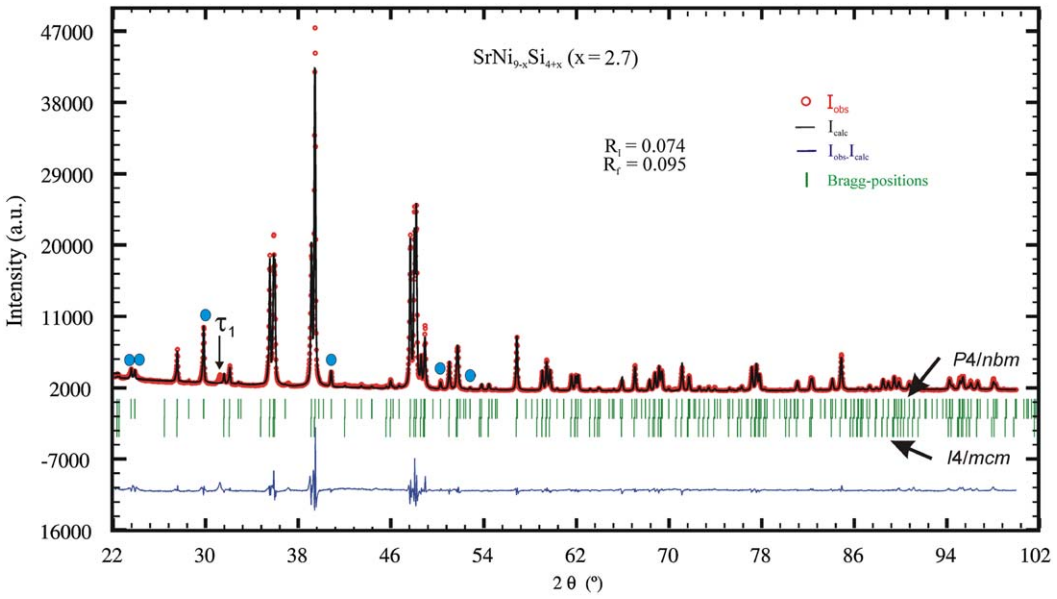

Fig. 5. Rietveld refinement of the X-ray powder diffraction profile for $SrNi_{9-x}Si_{4+x}$ (space group $P4/nbm$) in comparison with Bragg positions for space group $I4/mcm$. Prominent reflections of primitive cell are marked by blue dots. (For interpretation of the references to color in this figure legend, the reader is referred to the web version of this article.)

3.2.3. Ternary compounds with the $ThCr_2Si_2$-structure type (τ_2)

Inspection of a single crystal, isolated from melted sample with nominal composition $BaCd_2Ge_2$, reveals a body centered tetragonal unit cell. Structural solution by direct methods in the highest possible symmetry (space group *I*4/*mmm*) yielded three independent atom positions. For Ba-atoms in 2*a* (0, 0, 0), Cd in 4*d* $(0, \frac{1}{4}, \frac{1}{2})$ and Ge in the 4*e* (0, 0, *z*) sites, the structure successfully refines to R_{F2}=0.021 and a residual electron density 1.53 ē/Å^3 (see Table 3). X-ray Rietveld refinement for $BaZn_2Si_2$ confirms isotypism with $ThCr_2Si_2$ type (see Table 4).

The only free atom parameters $\sim 0.38 < z < \sim 0.39$ in combination with ratios $(2.3 < c/a < 2.5)$ for compounds $BaCd_2Ge_2$, $BaZn_2Si_2$, $BaZn_2Ge_2$, and $SrCu_{2-x}Si_{2+x}$ fit to the range observed for the majority of $ThCr_2Si_2$ type compounds [23] and were suggested to enable short Cr–Si ad Si–Si distances as also observed for $BaCd_2Ge_2$, $BaZn_2Si_2$, $BaZn_2Ge_2$, and $SrCu_{2-x}Si_{2+x}$.

3.2.4. Ternary compounds with the structure types related to $NaZn_{13}$ (τ_3)

Although binary $BaCu_{13}$ with cubic $NaZn_{13}$-type is known [22], no binary Sr–Cu homologue exists. The ternary system Sr–Cu–Si, however, reveals the formation of a cubic ternary phase τ_3'-$SrCu_{13-x}Si_x$ for $1.8 < x < 4$ (see Fig. 3). Rietveld refinement confirms structural identity with the $NaZn_{13}$-type (see Table 5). At a silicon content of $x \approx 4$ this phase undergoes a structural transformation into tetragonal τ_3-$SrCu_{9-x}Si_{4+x}$ with the $CeNi_{8.5}Si_{4.5}$ structure, which was already earlier established for x=0 from X-ray single crystal data [16]. The homogeneity region of τ_3-$SrCu_{9-x}Si_{4+x}$ at 800 °C extends up to x=1.0. In order to establish the atom site preferences for silicon-rich compositions of τ_3-$SrCu_{9-x}Si_{4+x}$, we performed X-ray Rietveld refinement for alloy with nominal composition x=1. These refinements reveal that the 4*d* site (occupied by Cu at x=0) is completely substituted by Si atom resulting in a composition $SrCu_{9-x}Si_{4+x}$ (x=1.0; R_F=0.054; R_I=0.078; Table 5).

An X-ray diffraction spectrum similar to tetragonal $SrCu_{9-x}Si_{4+x}$ is also observed for the ternary phase τ_3 in the Sr–Ni–Si system (Fig. 1). However, the X-ray profiles for single-phase compositions (Fig. 5) contain a set of reflections that do not belong to the $CeNi_{8.5}Si_{4.5}$-type structure (SG, *I*4/*mcm*). These reflections may be indexed in a primitive tetragonal unit cell. Single crystal fragments taken from samples within the homogeneity region of τ_3 confirm a primitive tetragonal structure with lattice parameter $a \approx 0.79$ nm and $c \approx 1.13$ nm, but in most cases twining along the *c*-axis was observed. Analysis of

Table 6
X-Ray single crystal and powder diffraction data for $SrNi_{9-x}Si_{4+x}$ (x=2.7) and $SrNi_{5.5}Si_{6.51}$ standardized with program *Structure Tidy* [31]. (Anisotropic displacement parameters [in 10^2nm^2]). $SrNi_{5.5}Si_{6.51}$

Parameter/compound	**$SrNi_{9-x}Si_{4+x}$ (x=2.7)** SC	**$SrNi_{5.5}Si_{6.5}\square_1$** XPD
Prototype	$SrNi_{9-x}Si_{4+x}$	$SrNi_{9-x}Si_{4+x}$
Space group	*P*4/*nbm*	*P*4/*nbm*
Composition, EMPA at.%	$Sr_{7.1}Ni_{50.7}Si_{40.2}$	$Sr_{7.1}Ni_{46.3}Si_{46.5}$
a ; c [nm], Ge standard	0.78998(3); 1.1337(2)	0.78528(5); 1.1213(1)
Reflections measured	$595 \geq 4\sigma(Fo)$ of 929	219
Θ range	$2 \leq 2\Theta \leq 70$; 250 s/frame	$8 \leq 2\Theta \leq 100$
Total number of frames	397; 9 sets	
Number of variables	47	34
Mosaicity	0.62	$R_F = \Sigma\lvert F_o - F_c\rvert/\Sigma F_o$ =0.074
$R_F^2 = \Sigma\lvert F_o^2 - F_c^2\rvert/\Sigma F_o^2$	0.036	$R_I = \Sigma\lvert I_o - I_c\rvert/\Sigma I_o$ =0.084
R_{Int}	0.079	$R_{wP}=[\Sigma w_i\lvert y_{oi}-y_{ci}\rvert^2/\Sigma w_i\lvert y_{oi}\rvert^2]^{1/2}$=0.048
wR2	0.086	$R_P = \Sigma\lvert y_{oi} - y_{ci}\rvert/\Sigma\lvert y_{oi}\rvert$=0.034
GOF	1.008	$R_e = [(N-P+C)/\Sigma w_i y_{oi}^2)]^{1/2}$ = 0.017
Extinction	0.000	$\chi^2 = (R_wP/R_e)2$ = 7.78
Residual density e−/Å^3; max; min	1.24; −1.66	–
Atom parameters		
Sr1 in 2*a* (1/4, 1/4, 0); Occ.	1.01(2)	1.00(1)
$U_{11}=U_{22};U_{33}$ / B_{iso}	0.0081(3); 0.0082(4)	1.4(1)
Sr2 in 2*b* (1/4, 1/4, 1/2); Occ.	1.00(1)	1.00(1)
$U_{11}=U_{22};U_{33}$ /B_{iso}	0.0083(3); 0.0087(4)	0.6(2)
M1 in 16n (*x*, *y*, *z*); *x*, *y*, *z*	0.05489(8), 0. 18943 (8), 0.25131(6)	0.0518 (3), 0.1913 (3), 0.2511(3)
U_{11}; U_{22}	0.0141(3); 0.0099(3)	B_{iso} =1.03(6)
U_{33}; U_{23}	0.0131(3); 0.0002(3)	–
U_{13}; U_{12}	0.0018(3); 0.0024(2)	–
Occ.	0.493(3)Ni + 0.507(3)Si	0.381(2)Ni + 0.619(2)Si
Ni1 in 8*m* (x, −x, z); x, z; Occ.	0.42424(6), 0.12135(7); 0.99(2)	0.4186(4), 0.1268(3)
$U_{11}=U_{22};U_{33}$	0.0132(2); 0.0229(4);	B_{iso} =2.59(7)
U_{23}= −U_{13};U_{12}	0.0021(2); -0.0023(3)	
Si1 8*m* (x, −x, z); x, z; Occ.	0.4194(1), 0.3698(1); 1.01(2)	0.4194(7), 0.3682(5)
$U_{11}=U_{22};U_{33}$	0.0129(4); 0.0135(7)	B_{iso}= 1.39(9)
U_{23}= −U_{13};U12	0.0029(4); −0.0053(5)	
Ni2 in 8*m* (x, −x, z); x, z; Occ.	0.62236(6), 0.42835(7); 0.99(2)	0.6260(4), 0.4257(3)
$U_{11}=U_{22};U_{33}$	0.0139(3); 0.0167(4)	B_{iso} =2.43(7)
U_{23}= −U_{13};U_{12}	0.0006(3); −0.0013(3)	
Si2 in 8*m* (x, −x, z); x, z; Occ.	0.6293(1), 0.0782(1); 1.01(2)	0.6256(6), 0.0861(5)
$U_{11}=U_{22};U_{33}$	0.0159(4); 0.0177(8)	B_{iso} =1.40(9)
U_{23}= −U_{13};U_{12}	0.0005(4); 0.0034(6)	–
M2 in 4h (¾, ¼, *z*); *z*	0.2499(2)	–
$U_{11}=U_{22};U_{33}$; U_{12}	0.0138(5); 0.0127(8); −0.0008(6)	–
Occ.	0.320(4)Ni + 0.680(4)Si	□

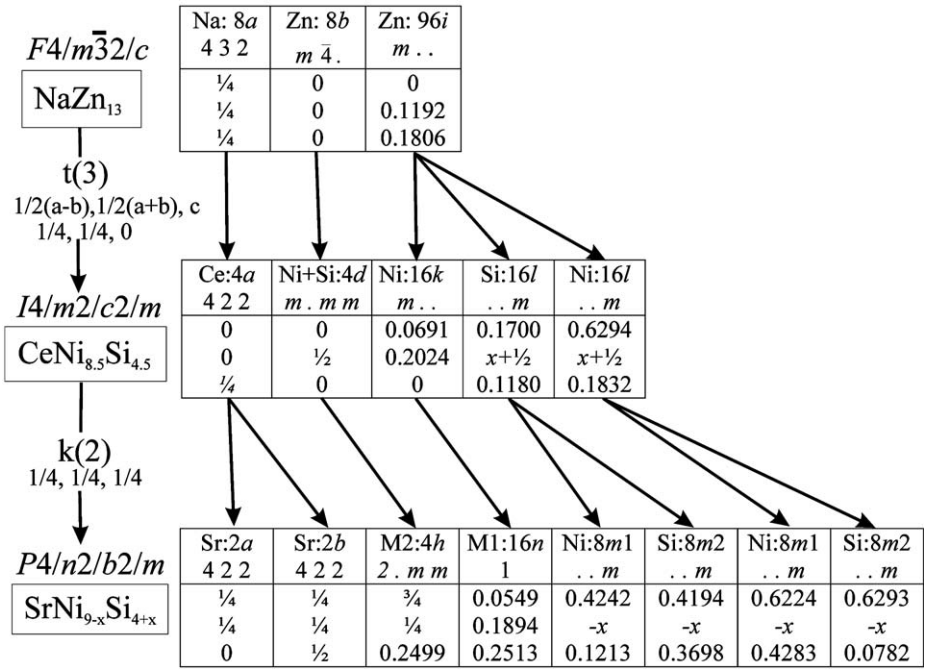

Fig. 6. Group–subgroup scheme in Bärnighausen formalism for $NaZn_{13}$ (*Fm*-3*c*) to $SrNi_{9-x}Si_{4+x}$ (*P*4/*nbm*).

the extinctions observed for an untwinned crystal ($a \approx 0.79$ nm and $c \approx 1.13$ nm) yields *P*4/*nbm* as the highest possible symmetry.

Structure solution via direct methods (Table 6) reveals an atomic arrangement similar to that for $SrCu_9Si_4$ (SG, *I*4/*mcm*), but with the difference that two 16*l* sites were found to be split into 8 fold positions (SG, *P*4/*nbm*) with almost complete atom order (Figs. 5 and 6). Refinement of the individual occupancies of all Wyckoff positions and temperature factors suggested a statistical distribution of Ni and Si atoms in sites 16*n* and 4*h* resulting in R_{F2}=0.036 and residual electron densities 1.24, and -1.66 e$^-$/Å^3. Only the occupancy of Si2 in the 8*m* site was found to be below 1.0. As substitution of about 6% Ni in this site does neither significantly change the R_{F2}-value (0.034) nor the anisotropic atom displacement parameters, complete ordering was kept for this site.

Although the structural solution obtained from the single crystal refinement describes very well the powder pattern for x=2.7 (Fig. 5), powder X-ray intensities significantly change for higher silicon contents due to changes in atom order. In order to investigate the site preference for the Si-rich boundary of τ_3, Rietveld refinement was performed for an alloy with nominal composition $Sr_{7.1}Ni_{41.9}Si_{51}$ (containing $<5\%$ of secondary Si). Rietveld analysis reveals a very small electron density in the 4*h* site (M2) in as cast state that corresponds to 0.55 Si atoms and a formula $SrNi_{5.8}Si_{6.3}\square_{0.9}$, whereas profile refinement of the annealed sample forced a complete disappearance of Si from the 4*h* site ($SrNi_{5.5}Si_{6.5}\square_1$, Table 6). The removal of the 4*h* site is also backed by the interatomic distances which become very small for $SrNi_{5.8}Si_{6.3}\square_{0.9}$ (d_{M2-Si}=0.20421 nm and d_{Si-Ni}=0.21043 nm) and finally for $SrNi_{5.5}Si_{6.5}\square_1$ d_{M2-Si}=0.19770 nm and d_{Si-Ni}=0.18557 nm. Although such deficiency has not been reported previously in any ternary variant of the $NaZn_{13}$-type or $CeNi_{8.5}Si_{4.5}$-type, a partial occupancy for the corresponding 8*b* site was recently established (see Fig. 6) for binary $AEZn_{13-x}$ (*AE*=Ca, Sr, Ba) [24] and $EuZn_{13-x}$ [25] ($x \approx 0.25$).

The group–subgroup relation among several structure variants of fcc-$NaZn_{13}$ has been shown in terms of a Bärnighausen tree [18,19] by Pöttgen and coworkers [26,27,28]. A new branch from $CeNi_{8.5}Si_{4.5}$ (S. G I4/mcm) leading to $SrNi_{9-x}Si_{4+x}$ (S. G. *P*4/*nbm*) via

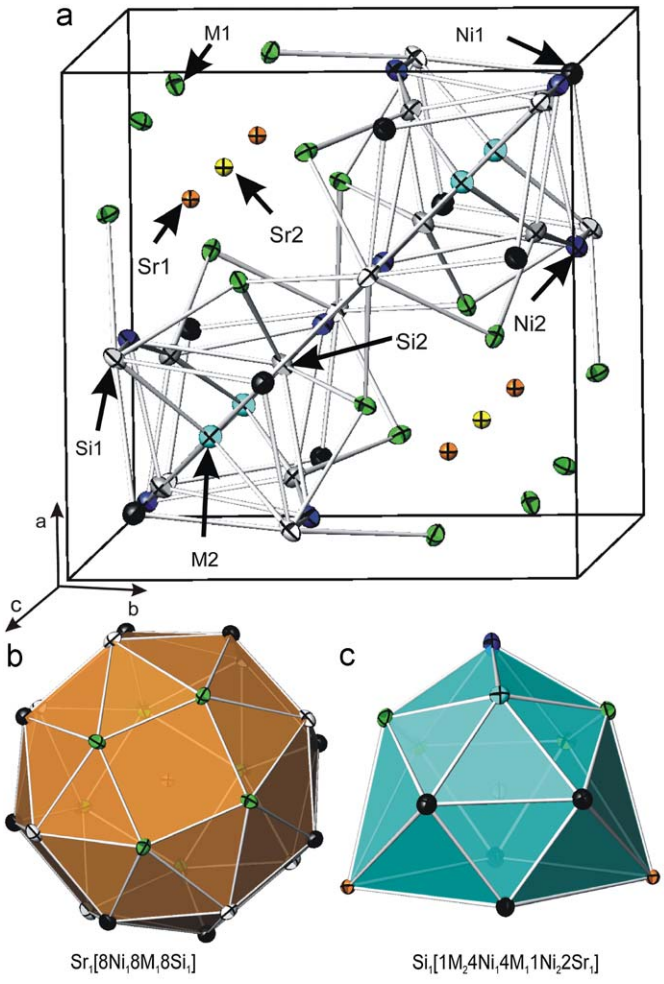

Fig. 7. (a) Crystal structure of $SrNi_{9-x}Si_{4+x}$ (space group *P*4/*nbm*) in three-dimensional view. Anisotropic thermal displacements from single crystal refinement. (b) Polyhedra around Sr1 and (c) Polyhedra around Si1.

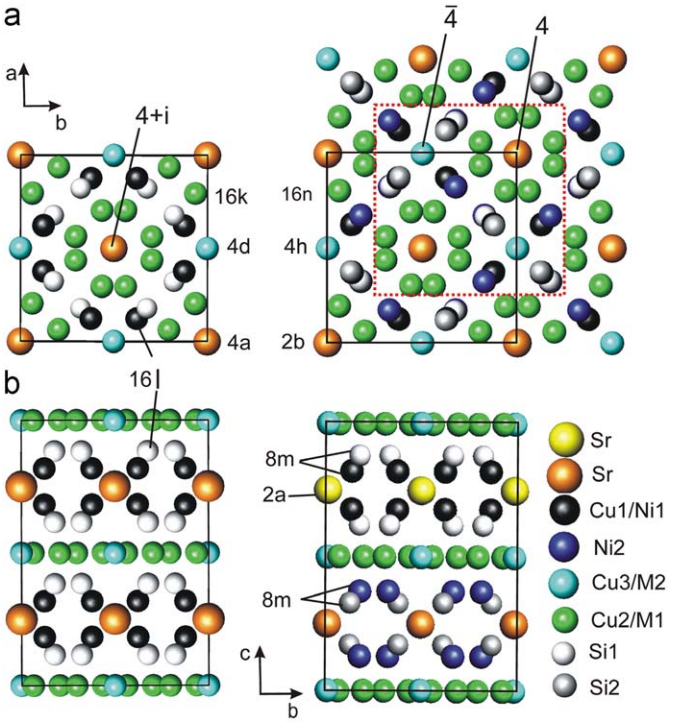

Fig. 8. Comparison of atom arrangements in $SrCu_{9-x}Si_{4+x}$ (space group *I*4/*mcm*) and $SrNi_{9-x}Si_{4+x}$ (space group *P*4/*nbm*) along *c*-axis (a) and along *a*-axis (b).

a *klassengleiche* symmetry reduction of index 2 is shown in Fig. 6. Atom arrangements in body centered and primitive tetragonal unit cells along *b*-axis and along *c*-axis are compared in Figs.7 and 8. It is easy to see that the atom arrangement in both structures is similar and a primitive super cell is the result of the splitting of two 16*l* sites. In going from *I*4/*mcm* to *P*4/*nbm* the mirror plane perpendicular to the 4-fold axis is changed to a diagonal glide plane *n* normal to the *c*-axis (see Fig. 8). The 4-fold axis with inversion center located at Sr (4*a*) in *I*4/*mcm* changes to a 4-fold axis located at Sr atoms (2*a* and 2*b*) and $\bar{4}$ located at M2 (4*h*) (origin choice 2 dotted) while the inversion center stays (Fig. 8a). Polyhedra around Sr and metal atoms are similar to those in $CeNi_{8.5}Si_{4.5}$-type with little distortion Fig. 7b and c.

4. Conclusion

Phase relations in the Sr-poor regions of the systems Sr–Ni–Si (at 900 °C) and Sr–Cu–Si (at 800 °C) were derived by X-ray diffraction, LOM and EPMA. Two new ternary compounds τ_2-$SrNiSi_3$ ($BaNiS_{n3}$-type), τ_3-$SrNi_{9-x}Si_{4+x}$ (own type) along with previously reported τ_1-$Sr(Ni_xSi_{1-x})_2$ (AlB_2-type) take part in the phase equilibria in Sr–Ni–Si. The structure of τ_3 $SrNi_{9-x}Si_{4+x}$ (own type) was solved by X-ray single crystal analysis and was found to be a primitive tetragonal variant of $NaZn_{13}$-type with space group *P*4/*nbm*. At higher Si-concentration defects are formed in the structure of $SrNi_{9-x}Si_{4+x}$. Three already known ternary compounds τ_1-$Sr(Cu_xSi_{1-x})_2$ (AlB_2-type), τ_2-$SrCu_{2-x}Si_{2+x}$ (x=0.16–0.44; $ThCr_2Si_2$-type), τ_3-$SrCu_{9-x}Si_{4+x}$($CeNi_{8.5}Si_{4.5}$-type) in Sr–Cu–Si were confirmed. Compositional polymorphism was observed for $SrCu_{13-x}Si_x$ ($1.8 \le x \le 4$) ($NaZn_{13}$-type) and $SrCu_{9-x}Si_{4+x}$ ($0 \le x \le 1.0$) ($CeNi_{8.5}Si_{4.5}$-type). Structural details were provided for numerous new compounds in the related systems Ba–*M*–X (*M*=Pd, Pt, Cu, Zn, Cd, Rh, Ir; *X*=Si, Ge).

Acknowledgments

The research reported herein was supported by the Higher Education Commission of Pakistan (HEC) under the scholarship scheme "PhD in Natural & Basic Sciences from Austria", and by the Austrian FWF projects P19165 and P16778-No2.

Appendix A. Supplementary material

Supplementary data associated with this article can be found in the online version at doi:10.1016/j.jssc.2009.12.023.

References

[1] N. Melnychenko-Koblyuk, A. Grytsiv, P. Rogl, M. Rotter, E. Bauer, G. Durand, H. Kaldarar, R. Lackner, H. Michor, E. Royanian, M. Koza, G. Giester, Phys. Rev. B Condens. Matter Mater. Phys. 14 (2007) 76.
[2] N. Melnychenko-Koblyuk, A. Grytsiv, P. Rogl, M. Rotter, R. Lackner, E. Bauer, L. Fornasari, F. Marabelli, G. Giester, Phys. Rev. B Condens. Matter Mater. Phys. 76 (2007) 195124.
[3] N. Melnychenko-Koblyuk, A. Grytsiv, P. Rogl, E. Bauer, R. Lackner, E. Royanian, M. Rotter, G. Giester, J. Phys. Soc. Jpn. 77 (2008) 54.
[4] A. Grytsiv, N. Melnychenko-Koblyuk, N. Nasir, P. Rogl, A. Saccona, H. Schmid, Int. J. Mat. Res. 100 (2009) 189.
[5] N. Melnychenko-Koblyuk, A. Grytsiv, L. Fornasari, H. Kaldarar, H. Michor, F. Rohrbacher, M. Koza, E. Royanian, E. Bauer, P. Rogl, M. Rotter, H. Schmid, F. Marabelli, A. Devishvili, M. Doerr, G. Giester, J. Phys. Condens. Matter 19 (2007) 26.
[6] N. Melnychenko-Koblyuk, A. Grytsiv, St. Berger, H. Kaldarar, H. Michor, F. Roehrbacher, E. Royanian, E. Bauer, P. Rogl, H. Schmid, G. Giester, J. Phys. Condens. Matter 19 (2007) 046203/1.
[7] N. Melnychenko-Koblyuk, A. Grytsiv, P. Rogl, H. Schmid, G. Giester, J. Solid State Chem. 182 (2009) 1754.
[8] A. Grytsiv, X.-Q. Chen, N. Melnychenko-Koblyuk, P. Rogl, E. Bauer, G. Hilscher, H. Kaldarar, H. Michor, E. Royanian, R. Podloucky, M. Rotter, G. Giester, J. Phys. Soc. Jpn. 77 (2008) 121.
[9] E. Bauer, R.T. Khan, H. Michor, E. Royanian, N. Melnychenko-Koblyuk, A. Grytsiv, P. Rogl, D. Reith, R. Podloucky, E.W. Scheidt, W. Wolf, M. Marsman, Phys. Rev. B: Condens. Matter Mater. Phys. 80 (2009) 064504.
[10] A. Grytsiv, P. Rogl, E. Bauer, H. Michor, E. Royanian, G. Giester, Intermetallics, 18 (2010) 173.
[11] N. Nasir, N. Melnychenko-Koblyuk, A. Grytsiv, P. Rogl, E. Bauer, E. Royanian, H. Michor, G. Hilscher, G. Giester, Intermetallics 17 (2009) 471.
[12] Nonius Kappa CCD Program Package COLLECT, DENZO, SCALEPACK, SORTAV, Nonius Delft, The Netherlands, 1998.
[13] G.M. Sheldrick, SHELXL-97 Program for Crystal Structure Refinement, University of Göttingen, Germany, 1997;
G.M. Sheldrick, Windows Version by McArdle, National University of Ireland, Galway, 1997.
[14] W. Rieger, E. Parthe, Monatsh. Chem. 100 (1969) 439.
[15] B. Eisenmann, N. May, W. Müller, H. Schäfer. A. Weiss, J. Winter, G. Ziegleder, Z. Naturforsch 25b (1970) 1350.
[16] C. Kranenberg, A. Mewis, Z. Anorg. Allg. Chem. 629 (2003) 1023.
[17] W. Dörrscheidt, H. Schäfer, J. Less-Common Met. 78 (1981) 69.
[18] H. Bärnighausen, Commun. Math. 9 (1980) 139.
[19] H. Bärnighausen, U. Müller, Symmetriebeziehungen zwischen den Raumgruppen als Hilfsmittel zur straffen Darstellung von Strukturzusammenhängen in der Kristallchemie, University of Karlsruhe and University, GH Kassel, 1996.
[20] W. Dörrscheidt, H. Schäfer, J. Less-Common Met. 58 (1978) 209.
[21] R. Demchyna, Yu. Prots, W. Schnelle, U. Burkhardt, U. Schwarz, Z. Kristallogr. NCS 221 (2006) 109.
[22] Pauling File Binaries Edition, Version 1.0, ASM International, Materials Park, OH, USA, release 2002/1.
[23] G. Just, P. Paufler, J. Alloys Compd. 232 (1996) 1.
[24] M. Wendorff, C. Röhr, J. Alloys Compd. 421 (2006) 24.
[25] B. Saparov, S. Bobev, J. Alloys Compd. 463 (2008) 119.
[26] V. Zaremba, I.R. Muts, R.-D. Hoffman, R. Pöttgen, Z. Anorg. Allg. Chem. 629 (2003) 2330.
[27] Y. M. Kalychak, V. Zaremba, Y. V. Galadzhun, K. Y. Miliyanchuk, R.-D. Hoffmann, R. Pöttgen, Chem. Eur. J. 7 (2001) 5343.
[28] R.-D. Hoffmann, I. Muts, V. Zaremba, R. Pöttgen, Z. Kristallogr. 224 (2009) 446.
[29] D.M. Proserpio, G. Artioli, S. Mulley, G. Chacon, C. Zneng, Chem. Mater. 9 (1997) 1463.
[30] O.I. Bodak, E.I. Gladyshevskii, Dopovidi Akademii Nauk Ukrains's Koi RSR Seryia A: Fiziko-Tekhnichni ta Matermatichni Nauki 30 (1968) 944.
[31] E. Parthe', L. Gelato, B. Chabot, M. Penzo, K. Cenzual, R. Gladyshevskii, TYPIX Standardized Data and Crystal Chemical Characterization of Inorganic Structure Types, Springer, Berlin, Heidelberg, 1994.